Zone-boundary phonons in hexagonal and cubic GaN

H. Siegle, G. Kaczmarczyk, L. Filippidis, A. P. Litvinchuk, A. Hoffmann, and C. Thomsen
Institut für Festkörperphysik, Technische Universität Berlin, 10623 Berlin, Germany
(Received 26 August 1996; revised manuscript received 8 November 1996)

We present results of second-order Raman-scattering experiments on hexagonal and cubic GaN covering the acoustic and the optical overtone spectral region. Based on a comparison of the experimental scattering data with the calculated phonon-dispersion curves as well as the group-theoretically derived selection rules, we were able to assign the observed structures to particular phonon branches and determined the points in the Brillouin zone from which the scattering originates. Our measurements reveal the energies of acoustic zone-boundary phonons in hexagonal GaN. [S0163-1829(97)01812-2]

I. INTRODUCTION

The wide-band-gap semiconductor GaN has attracted considerable attention over the past years because of its interesting physical properties and its application as a basic material for optoelectronic devices working in the blue and ultraviolet spectral region.[1] In spite of impressive technological achievements in the past few years culminating in the very recent realization of the first GaN-based laserdiode[2] relatively little is known about the basic physical properties compared to other III-V semiconductors. Only little effort has been made to analyze the lattice dynamics of GaN. Since large enough single crystals of GaN of sufficient quality are not yet available for neutron-scattering studies we performed second-order Raman-scattering experiments on hexagonal and on cubic GaN. In contrast to first-order Raman measurements second-order experiments provide information on the vibrational states throughout the entire Brillouin zone, which is important in considering, for example, the electronic conduction or the nonradiative relaxation processes of electrons.

Up until now the only publication about second-order Raman scattering on GaN known to the authors is Ref. 3. Murugkar *et al.* have investigated hexagonal GaN for frequencies higher than 1280 cm^{-1}; no assignment has been made until now.

We present a comprehensive study of second-order Raman scattering on both modifications of GaN, hexagonal, and cubic. We used all necessary scattering geometries to obtain selection rules and performed a calculation of the dispersion curves. The spectral region investigated contains the acoustic as well as the optical overtone and combination part. Thus, we obtained the energies of zone-boundary acoustic phonons in GaN. In order to derive the selection rules for second-order Raman scattering we performed a group-theoretical analysis. Using these selection rules in addition to the calculated dispersion curves we assigned the observed peaks to particular phonon branches and determined the points in the Brillouin zone from which the scattering originates.

II. EXPERIMENT

The samples investigated were about 1-μm-thick layers of cubic GaN grown on (001) GaAs by molecular-beam epitaxy (MBE) and 200–400-μm-thick hexagonal layers grown on sapphire using hydride vapor phase epitaxy (HVPE). The Raman-scattering experiments were carried out using a Dilor LABRAM single-grating spectrometer with a charge-coupled device (CCD) detector and confocal optics. The spectral resolution was about 1 cm^{-1}. The samples were excited either perpendicular or parallel to the substrate surface depending on the scattering geometry using the 632.8-nm line of a He-Ne laser and the 514.53-nm line of an Ar^+ laser. By passing the laser through a microscope objective ($\times 80$ or $\times 100$) the laser beam was focused on a point spot with a diameter of about 1 μm. The scattered light was detected in backscattering geometry which corresponds to either an $x(zz)\overline{x}\ (A_1)$, an $x(yz)\overline{x}\ (E_1)$, or a $z(xy)\overline{z}\ (E_2)$ configuration. Temperature-dependent measurements in the range between 4.2 and 330 K were performed using an Oxford microscope cryostat.

It is noteworthy that none of the structures observed in the following Raman spectra of the hexagonal samples are caused by the sapphire substrate[4] because of the microscope and confocal optics used. They allow the restriction of the focal depth to 2–10 μm depending on the objective used and efficiently eliminate any signals from the substrate. On the other hand, we compared our spectra with measurements taken on hexagonal GaN grown on SiC. We obtained the same results on several differently prepared samples.

III. THEORETICAL MODEL

We used a modified valence-force model of Kane[5] to calculate the phonon-dispersion curves of hexagonal GaN. First the dynamical matrix was set up and diagonalized numerically which yields the eigenmodes for different **k** vectors. The elastic potential used for the calculation consisted of five valence-force potentials and one Coulomb term, which describes the long-range forces due to Coulomb interactions in ionic crystals (effective-charge parameter Z^*, Table I). The valence-force potentials describe the bond stretching and bond bending (force-constant parameters α and β, respectively) of the nearest and next-nearest neighbors and the MSBN (Ref. 6) interaction, i.e., bond-bending forces between three adjacent lattice bonds (force-constant parameter μ). The anisotropy of hexagonal GaN was taken into account by introducing two sets of parameters: one describing inter-

TABLE I. Nearest-neighbor and MSBN (Ref. 6) parameters (in meV/Å^2) of GaN, AlN, and ZnO used in our modified valence-force model. Z^* is the effective charge parameter. The force-constant parameters α, β, and μ are each subdivided into one parameter describing interactions perpendicular to the c axis and one parallel to the c axis (index C), respectively. The indices 1 and 2 of the parameter β indicate the different bond-bending configurations, i.e., whether the nitrogen (oxygen) (1) or the group-III element (zinc) (2) are displaced.

Material	Z^*	α	α_C	β_1	β_{1C}	β_2	β_{2C}	μ	μ_C
GaN	1.124	4.680	4.361	−0.693	−0.519	1.341	1.004	−0.087	−0.024
AlN	1.226	5.381	5.606	−0.690	−0.356	1.254	0.646	−0.104	−0.062
ZnO	1.048	3.089	3.555	−1.132	−1.150	1.502	1.526	−0.024	−0.037

actions along the c axis and one for interactions perpendicular to the c axis.[7]

We started the calculation by using the Kane parameters of ZnO, which has similar structural and lattice-dynamical properties as GaN and AlN. By adjusting our model to results of *ab initio* calculations of AlN (Ref. 8) we obtained corresponding results. With the knowledge of the parameters for both materials, ZnO and AlN, we had starting values to calculate the phonon dispersion of GaN and could adjust our model to the values obtained by our Raman-scattering experiments. The main parameters used for our calculations are listed in Table I.

IV. RESULTS AND DISCUSSION

GaN exists in both modifications cubic and hexagonal which differ in packing sequence only (cubic: *ABCABC*; hexagonal: *ABAB*). Hexagonal GaN grows in the wurtzite structure and belongs to the point group C_{6v} (6 mm) having four atoms per unit cell. Near $\mathbf{k}=\mathbf{0}$ group theory predicts the following eight sets of modes: $2A_1+2B+2E_1+2E_2$ from which one A_1, one E_1 and two E_2 are Raman active. One set of A_1 and one E_1 corresponds to acoustic phonons. The B modes are silent.[9] Cubic GaN has zinc-blende structure and belongs to the point group T_d ($43m$) having two atoms per primitive unit cell and thus six phonon branches. Near the Γ point the acoustic phonons have $T_1=\Gamma_{25}$ symmetry and the optical phonons have $T_2=\Gamma_{15}$ symmetry. The optical modes which may be easily seen by first-order Raman scattering are a doubly degenerate TO and a single LO phonon with a higher frequency.[9] The frequencies of the first-order Raman modes of hexagonal GaN are listed in Table III together with the second-order frequencies.

A. Group-theoretical selection rules for second-order Raman scattering

In second-order Raman scattering experiments the momentum conservation does not restrict the range of phonon wave vectors taking part in the scattering as is the case in first-order scattering. Instead, phonons with wave vectors throughout the whole Brillouin zone are involved. Thus, the second-order intensity reflects the phonon density of states, which in turn is related to the phonon dispersion. The various structural characteristics of the second-order spectra are due largely to variations in the density of phonon states and selection rules for the various scattering processes (combinations and overtones).

While the selection rules for second-order Raman-scattering processes in cubic materials are well known and were already applied to the assignment of spectral features in the second-order spectra, only sparse information is found in the literature about the selection rules for second-order scattering in hexagonal materials.[10] Therefore, we performed a group-theoretical analysis and summarized the results in Table II. From this table the following conclusions can be drawn:

(i) Overtones always contain the representation A_1 while combinations of phonon states belonging to different irreducible representations never contain A_1.

(ii) More overtones or combinations become allowed with decreasing symmetry of the point in the Brillouin zone considered.

(iii) A consequence of the different packing sequence of hexagonal GaN compared to cubic material is halving of the Brillouin-zone dimension in the cubic (111) direction, which is followed by a folding of the phonon branches at the new zone boundary. Frequencies which previously occurred at the symmetry point L in the zinc-blende Brillouin zone now occur at the center of the wurtzite Brillouin zone. Consequently the different phonon branches from the Γ point, e.g., the optical $\Gamma_6=E_2$ and the acoustic $\Gamma_3=B$ run together at the A point. Therefore we use $A_{\mathrm{I}}=A_1+A_3$ and $A_{\mathrm{II}}=A_5+A_6$. The same is valid for the H and L point. It is important to note also that, apart from the selection rules, the density of two-phonon states determines the intensity of the second-order Raman signal.[9]

B. Second-order Raman spectra of hexagonal and cubic GaN

Figure 1 shows an overview of a room-temperature second-order Raman spectrum of a hexagonal (upper curve) and a cubic (bottom curve) GaN layer taken in $z(\ )\bar{z}$ geometry (corresponding to A_1+E_2). Apart from the strong first-order modes at 569 cm^{-1} (E_2) and at 735 cm^{-1} (A_1(LO)) of the hexagonal material[11–13] and at 555 cm^{-1} (TO) and 742 cm^{-1} (LO) of the cubic material[13] a rich structure due to second-order scattering processes can be seen.

The total spectrum may be divided into three parts: the low-frequency region of the spectra (approximately 200–650 cm^{-1}) is dominated by acoustic overtones; optical and acoustic combination bands (650–1000 cm^{-1}) appear below and above the first-order optical scattering; and, finally, the second-order optical bands lie in the high-frequency portion of the spectra (1000–1500 cm^{-1}). The corresponding spectra taken from hexagonal GaN in A_1, E_1, and E_2 scattering ge-

TABLE II. Group-theoretical selection rules for two-phonon Raman scattering in crystals with a wurtzite structure.

Point in the Brillouin zone; corresponding symmetry	Irreducible representations for points in the Brillouin zone and their correlations	Overtones	Combinations
$\Gamma;C_{6V}$	$A_1=\Gamma_1$	$[\Gamma_1]^2,[\Gamma_3]^2\supset A_1$	$\Gamma_1\times\Gamma_1,\Gamma_3\times\Gamma_3\supset A_1$
	$B_1=\Gamma_3$	$[\Gamma_5]^2,[\Gamma_6]^2\supset A_1,E_2$	$\Gamma_5\times\Gamma_5,\Gamma_6\times\Gamma_6\supset A_1,E_2$
	$E_1=\Gamma_5$		$\Gamma_1\times\Gamma_5,\Gamma_3\times\Gamma_6,\Gamma_5\times\Gamma_6\supset E_1$
	$E_2=\Gamma_6$		$\Gamma_1\times\Gamma_6,\Gamma_3\times\Gamma_5\supset E_2$
$A;C_{6V}$	$\Gamma_i\rightarrow A_i$	$[A_{\mathrm{I}}]^2\supset A_1$	$A_{\mathrm{I}}\times A_{\mathrm{I}}\supset A_1$
	$A_{\mathrm{I}}=A_1+A_3$	$[A_{\mathrm{II}}]^2\supset A_1,E_1,E_2$	$A_{\mathrm{II}}\times A_{\mathrm{II}}\supset A_1,E_1,E_2$
	$A_{\mathrm{II}}=A_5+A_6$		$A_{\mathrm{I}}\times A_{\mathrm{II}}\supset E_1,E_2$
$K;C_{3V}$	$A_1\rightarrow K_1$	$[K_1]^2,[K_2]^2\supset A_1$	$K_1\times K_1,K_2\times K_2\supset A_1$
	$B_1\rightarrow K_2$	$[K_3]^2\supset A_1,E_2$	$K_3\times K_3\supset A_1,E_1,E_2$
	$E_1\rightarrow K_3$		$K_1\times K_3,K_2\times K_3\supset E_1,E_2$
	$E_2\rightarrow K_3$		
$H;C_{3V}$	$H_1=H_1+H_2$	$[H_1]^2\supset A_1$	$H_1\times H_1\supset A_1$
	H_3	$[H_3]^2\supset A_1,E_1$	$H_3\times H_3\supset A_1,E_1,E_2$
			$H_1\times H_3\supset E_1,E_2$
$M;C_{2V}$	$A_1\rightarrow M_1$	$[M_1]^2,[M_2]^2\supset A_1,E_2$	$M_i\times M_i\supset A_1,E_2$
	$E_1\rightarrow M_3+M_4$	$[M_3]^2,[M_4]^2\supset A_1,E_2$	$M_1\times M_2,M_3\times M_4\supset E_2$
	$E_2\rightarrow M_1+M_2$		$M_1\times M_3,M_1\times M_4\supset E_1$
			$M_2\times M_3,M_2\times M_4\supset E_1$
$L;C_{2V}$	$L_{\mathrm{I}}=L_1+L_3$	$[L_{\mathrm{I}}]^2,[L_{\mathrm{II}}]^2\supset A_1,E_1,E_2$	$L_{\mathrm{I}}\times L_{\mathrm{I}},L_{\mathrm{II}}\times L_{\mathrm{II}}\supset A_1,E_1,E_2$
	$L_{\mathrm{II}}=L_2+L_4$		$L_{\mathrm{I}}\times L_{\mathrm{II}}\supset E_1,E_2$

ometry are shown in Figs. 2(a)–2(c). The frequencies of the observed second-order Raman features together with the observed symmetries and their assignments are listed in Table III. In the following we discuss for each region the strongest experimentally observed structures along with our calculated phonon-dispersion curves for hexagonal GaN (see Fig. 3) and compare them with modes observed in cubic GaN.

Low-frequency region: Acoustic overtones

The low-frequency region shown in Fig. 2(a) exhibits two strong Raman bands, one located at 317 cm^{-1} and a doublet at 410/420 cm^{-1}. The temperature dependence of their intensities follows closely the one expected for second-order scattering processes.[9] The 317- and the 410-cm^{-1} modes clearly have A_1 symmetry. The 420-cm^{-1} mode also shows E_2 symmetry [see inset of Fig. 2(a)].

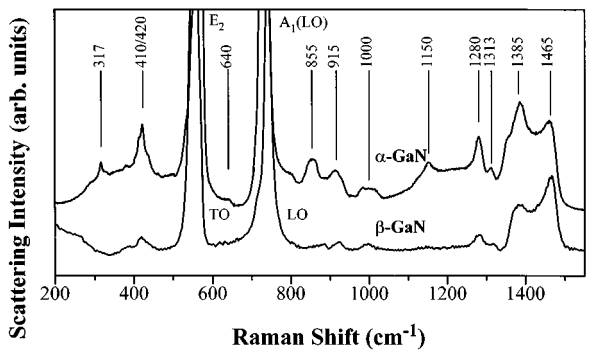

FIG. 1. Second-order Raman spectrum of hexagonal (upper curve) and cubic (bottom curve) GaN grown on (0001) sapphire and (001) GaAs, respectively. The spectra were recorded at room-temperature in backscattering geometry, corresponding to $z(\ )\overline{z}$.

From the lineshape and from its low frequency we can assign the 317-cm^{-1} mode to an overtone process of acoustic phonons. As can be seen in the calculated phonon-dispersion curves (Fig. 3) the energy position as well as the observed symmetry fits well with the flat phonon branch at the H point in the Brillouin zone. This is emphasized by the fact that this mode was not observed in cubic GaN.

The doublet around 415 cm^{-1} is also due to acoustic phonons. Comparing the calculated phonon-dispersion curves in Fig. 3 as well as the curves of ZnO (Ref. 14) and AlN (Ref. 8) the doublet in question can be attributed to an overtone of transverse-acoustic phonons either at the symmetry point A, K, or M in the Brillouin zone. The energy posi-

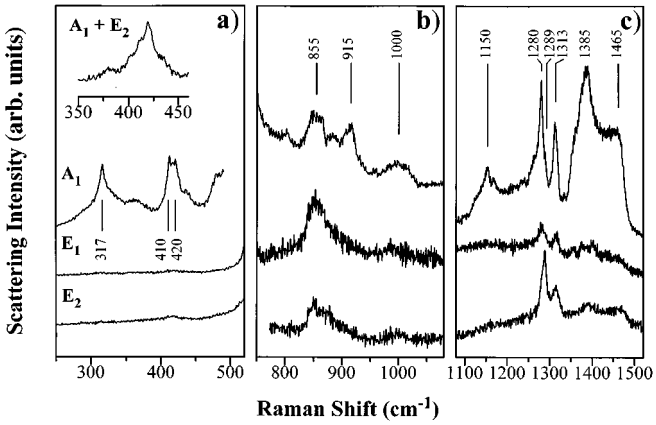

FIG. 2. Second-order room-temperature Raman spectra of the hexagonal sample taken at room temperature for various scattering geometries corresponding to symmetry A_1, E_1, and E_2 in the (a) low-, (b) middle-, and (c) high-frequency region. Excitation was at 632.8 nm.

TABLE III. Frequencies (in cm^{-1}) and symmetries of the strongest modes found in the second-order Raman spectra of hexagonal GaN and their assignments.

Frequency (cm^{-1})	Symmetry	Process	Point in the BZ
317	A_1	acoust. overtone	H
410	A_1	acoust. overtone	A,K
420	A_1,E_2	acoust. overtone	M
533	A_1	first-order process	$\Gamma=A_1$(TO)
560	E_1	first-order process	$\Gamma=E_1$(TO)
569	E_2	first-order process	$\Gamma=E_2$ (high)
640	A_1	overtone	$\Gamma=[B]^2,L$
735	A_1	first-order process	$\Gamma=A_1$(LO)
742	E_1	first-order process	$\Gamma=E_1$(LO)
855	A_1,E_1,E_2	acust.-opt. comb.	
915	A_1	acust.-opt.comb.	
1000	$A_1,(E_2)$	acust.-opt. comb.	
1150	A_1	opt. overtone	
1280	$A_1,(E_1)$	opt. comb.	
1289	E_2	opt. comb.	
1313	$A_1,(E_1,E_2)$	opt. comb.	
1385	A_1	opt. overtone	A,K
1465	A_1	opt. overtone	$\Gamma=[A_1,\mathrm{LO}]^2$
cutoff 1495	A_1,E_2	opt. overtone	$\Gamma=[E_1,\mathrm{LO}]^2$

tion as well as the symmetry expected from the group-theoretical selection rules (Table II fit together with the experimental observation. In addition, the dispersion curve runs flat at these points, consequently the density of phonon states is high. According to Table II) we can attribute the lower-energy mode located at 410 cm^{-1} which exhibits A_1 symmetry to the A or K point while the higher-energy portion of the doublet belongs to the M point. At this point an overtone of transverse-acoustic phonons has A_1 and E_2 symmetry. The small energy difference of 10 cm^{-1} between these points is also observed in the dispersion curves of ZnO (Ref. 14) and AlN.[8] As can be seen in Fig. 1 this mode was also observed in cubic GaN. The hexagonal mode lying between the first-order peaks at around 640 cm^{-1} can be attributed to an overtone process of the highest acoustic-phonon branch either at the zone boundary (L point) or from the B mode at the Γ point.

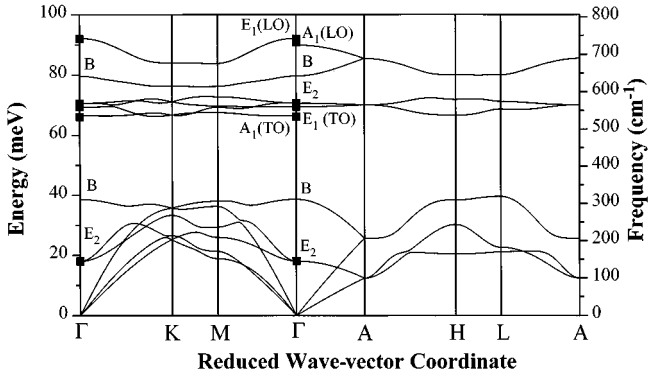

FIG. 3. Calculated phonon-dispersion curves for hexagonal GaN.

Middle-frequency region: Acoustic and optical combinations

In Fig. 2(b) the middle-frequency region is plotted. This region exhibits a rich structure of less intensive modes. The strongest features are the structures around 855, 915, and 1000 cm^{-1}. Except for the mode around 855 cm^{-1} all modes have well-defined A_1 symmetry; the mode around 1000 cm^{-1} may have additionally E_2 symmetry. The 855 cm^{-1} mode was only detected in hexagonal GaN. We attribute all these modes to second-order Raman-scattering processes, but we were only able to make a tentative assignment of these peaks. Considering the phonon-dispersion curves in Fig. 3 and the fact that most of these structures are also found in the spectra taken from cubic samples, it becomes clear that only combinations between acoustic and optical phonons can provide the frequency found experimentally. Because of the gap between the acoustic- and optical-phonon branches, which extends in the overtone spectrum from approximately 650–1050 cm^{-1}, overtones can be excluded.

High-frequency region: Optical combinations and overtones

The optical combination and overtone region is shown in Fig. 2(c). Most of the modes observed in this region were strongest in A_1 symmetry.

The structure located at 1150 cm^{-1} is probably a consequence of the flatness of the dispersion curve of GaN in the energy region between the A_1(TO)=533 cm^{-1} and E_2=569 cm^{-1} as the comparison with the calculated dispersion curves in Fig. 3 or with the dispersion curves of ZnO (Ref. 14) or AlN (Ref. 8) shows. From the observed A_1 symmetry and according to the selection rules in Table II we infer a second-order process from the K or the H point in the Brillouin zone. Although the dispersion curve is also flat at the Γ and A point overtone or combination processes at these

points can be excluded because such processes should have A_1, E_2 (overtones) or A_1, E_2, or E_1 (combination tones) symmetry at the Γ point and A_1, E_1, E_2 symmetry at the A point. This assignment is correct only under the assumption that the scattering cross section does not vary strongly for the different symmetries.

As is the case in other hexagonal or cubic semiconductors the highest-frequency second-order Raman signal originates from optical-phonon overtones.[10,15,16] In GaN this region is dominated by two relatively narrow peaks at 1280 and 1313 cm^{-1} and a camelback-like structure lying between 1340 and 1495 cm^{-1} with maxima at 1385 and 1465 cm^{-1} and a shoulder at 1350 cm^{-1}. In the following we will discuss these peaks starting with the structure highest in energy and proceeding toward lower energies.

The highest-energy distribution of the second-order Raman signal with a cutoff at 1495 cm^{-1} is attributed to an overtone of the zone-center E_1(LO) mode. Apart from the good agreement of the expected (1482 cm^{-1}) and observed (1495 cm^{-1}) energies also the predicted A_1 and E_2 symmetry were observed [Fig. 2(c)]. The upper maximum of the camelback structure at around 1465 cm^{-1} corresponds to an overtone of the zone-center A_1(LO) mode. The lower camelback at 1385 cm^{-1} together with its shoulder at 1350 cm^{-1} arises from the highest phonon branches which become flat at the Brillouin-zone boundary. Scattering processes originating from either the A point, where the corresponding phonon branch runs extremely flat in direction to the H point, or from the K point are possible considering both energy and predicted symmetry. We found the camelback structure also in cubic GaN so a scattering process at the A point can be excluded.

We discuss now the two narrow peaks at 1280 and 1313 cm^{-1}. Both are extremely intense in A_1 symmetry but also detectable in E_1 symmetry. In the E_2 spectrum the 1313-cm^{-1} mode can also been seen but instead of the 1280-cm^{-1} peak a mode appears at 1289 cm^{-1}. Although combinations of the zone-center A_1(TO), A_1(LO), E_1(TO), and E_1(LO) modes are possible from energy considerations, the experimentally observed symmetry does not correspond to those expected from group-theoretical consideration and one cannot explain their appearance in the cubic spectra (Fig. 1). Most probably these modes are caused by combination processes at the zone boundary. The high-energy phonon branch involved is the one from which the lower cutoff of the camelback structure originates due to an overtone process as already described above. The other phonons involved belong to the flat phonon branches which form at the zone center the A_1(TO), E_1(TO), and E_2 modes.

V. SUMMARY

We presented second-order Raman-scattering results of cubic and hexagonal GaN. We assigned most of the observed structures in the spectra to particular phonon branches and determined the points in the Brillouin zone from which the scattering originates. For this we have compared the experimentally observed energy positions and the symmetry behavior of the modes with the selection rules derived by a group-theoretical analysis and the phonon-dispersion curves calculated by a modified valence-force model of Kane.

ACKNOWLEDGMENTS

We thank D. Schikora, M. Hankeln, and K. Lischka for supplying the cubic samples and T. Detchprohm and K. Hiramatsu for the hexagonal samples which were used in these experiments. We also thank C. Göbel and U. Scherz for useful discussions.

[1] R. F. Davis, Proc. IEEE **79**, 702 (1991); S. Strite and H. Morkoç, J. Vac. Sci. Technol. B **10**, 1237 (1992).
[2] S. Nakamura, Jpn. J. Appl. Phys. **35**, L74 (1996).
[3] S. Murugkar, R. Merlin, A. Botchkarev, A. Salvador, and H. Morkoc, J. Appl. Phys. **77**, 6042 (1995).
[4] For a survey of Raman spectra on sapphire see, for example, S. P. S. Porto and R. S. Krishnan, J. Chem. Phys. **47**, 1009 (1967).
[5] E. O. Kane, Phys. Rev. B **31**, 7865 (1985).
[6] H. L. McMurry, A. W. Solbrig, J. K. Boyter, and C. Noble, J. Phys. Chem. Solids **28**, 2359 (1967).
[7] P. Thurian, G. Kaczmarczyk, H. Siegle, R. Heitz, A. Hoffmann, I. Broser, B. K. Meyer, R. Hoffbauer, and U. Scherz, Proceedings of the 18th International Conference on Defects in Semiconductors [Mater. Sci. Forum. **196–201**, 1571 (1995)].
[8] K. Karch, G. Portisch, F. Bechstedt, P. Pavone, and D. Strauch, Inst. Phys. Conf. Ser. No. **142**, 967 (1996).
[9] M. Cardona, in *Light Scattering in Solids II*, edited by M. Cardona and G. Güntherodt, Topics in Applied Physics Vol 50 (Springer, Berlin, 1982), p. 19 ff.
[10] I. S. Gorban and V. I. Lugovoi, Zh. Prikl. Spektrosk. **24**, 333 (1976).
[11] D. D. Manchon, A. S. Barker, P. J. Dean, and R. B. Zetterstrom, Solid State Commun. **8**, 1227 (1970).
[12] T. Kozawa, T. Kachi, H. Kano, Y. Taga, and M. Hashimoto, J. Appl. Phys. **75**, 1098 (1994).
[13] H. Siegle, L. Eckey, A. Hoffmann, C. Thomsen, B. K. Meyer, D. Schikora, M. Hankeln, and K. Lischka, Solid State Commun. **96**, 943 (1995).
[14] A. W. Hewat, Solid State Commun. **8**, 187 (1970).
[15] P. A. Temple and C. E. Hathaway, Phys. Rev. B **7**, 3685 (1973).
[16] B. A. Weinstein and M. Cardona, Phys. Rev. B **7**, 2545 (1973).